NJC

PAPER

View Article Online
View Journal | View Issue

Check for updates

Cite this: *New J. Chem.*, 2017, **41**, 10009

A family of solution-processable macrocyclic and open-chain oligothiophenes with atropoisomeric scaffolds: structural and electronic features for potential energy applications†

E. Quartapelle Procopio,[a] T. Benincori,[b]* G. Appoloni,[b] P. R. Mussini,[a] S. Arnaboldi,[a] C. Carbonera,[c] R. Cirilli,[d] A. Cominetti,[c] L. Longo,[c] R. Martinazzo,[a] M. Panigati[ae] and R. Pò[c]*

Received 4th May 2017,
Accepted 25th July 2017

DOI: 10.1039/c7nj01501a

rsc.li/njc

$FeCl_3$ oxidation of the racemate of C_2 symmetric, inherently chiral, sexithiophene monomer **1** (2,2′-bis(2,2′-bithiophene-5-yl)-3,3′-bithianaphthene) affords a mixture of cyclic oligomers, from the prevailing dimer to traces of the pentamer. The oligomers are constituted by mixtures of stereoisomers which are two for dimer **2**, four for trimer **3** and six for tetramer **4**. Cyclooligomers **2** and **3** could be separated by chromatography, while **4** was synthesized by ring closure of open chain dimer **2a**, prepared in turn by controlled coupling of the anion of racemic **1**. The optical properties of open-chain stereoisomer **2a** and tetramer **4** have been compared with those of **2** and **3** respectively. The macrocyclic oligomers have been tested as donor materials in bulk heterojunction solar cell prototypes both as a crude mixture resulting from oxidation of **1** and as a single oligomer. Theoretical calculations support the photophysical properties of these new materials.

Published on 26 July 2017. Downloaded by Universita Studi di Milano on 6/8/2022 8:42:27 AM.

Introduction

Conjugated oligothiophene macrocycles are attracting increasing scientific interest due to some peculiar properties related to their cyclic structure:[1–6] (i) they idealize conducting polymers without ends which generally represent the weak point of conducting materials; (ii) they are soluble in many aprotic organic solvents, unlike α-oligothiophenes which display very serious solubility problems; (iii) they offer electrosensitive cavities of different sizes[1] for selective inclusion of guest molecules;[7] (iv) they allow the tuning of the self-assembling process in the condensed phase;[8] (v) the modern synthetic strategies involving synthons endowed with suitably oriented thiophene termini are very efficient and competitive with those employed to accede to linear oligothiophene systems.[9,10]

We have recently reported that $FeCl_3$ oxidation of the enantiopure antipodes of the inherently chiral sexithiophene monomer **1** (2,2′-bis(2,2′-bithiophene-5-yl)-3,3′-bithianaphthene) affords a mixture of cyclic oligomers from which enantiopure symmetric dimer **2** and trimer **3** (having D_2 and D_3 symmetry respectively) have been separated in the pure state by column chromatography (Scheme 1).[11]

In these molecules the same conjugated system responsible for optical and electrochemical properties is also responsible for molecular chirality, implying that the chiroptical and the enantiorecognition properties of the material are strictly correlated with the electrochemical ones.[11,12] Indeed, films of the dimers and trimers show outstanding chiroptical properties [CD, rotatory power and Circularly Polarized Luminescence (CPL)], an electrochemical behaviour similar to that exhibited by stable polythiophenes (PTs),[13,14] and an unimaginable enantiorecognition ability towards the enantiomers of different chiral probes, both as single enantiomers and as racemates.[15]

Since **2** and **3** are not the exclusive products, in this paper we report the results of the investigation on the properties of the whole materials resulting from the chemical oxidation of racemic **1**, evaluating also the stereoisomer distribution for the different macrocycles. Furthermore, we investigated the possibility of employing selected mixtures of macrocyclic oligothiophene stereoisomers as donors in bulk-heterojunction solar cells (BHJSCs), and the overall efficiencies of the resulting

[a] *Università di Milano, Dip. di Chimica and C.I.Ma.I.NA, via Golgi 19, 20133 Milano, Italy. Fax: +39 02-50314139*
[b] *Dip. di Scienza e Alta Tecnologia, Università degli Studi dell'Insubria, via Valleggio 11, 22100 Como, Italy. E-mail: tiziana.benincori@uninsubria.it*
[c] *Renewable Energies & Environmental R&D, Istituto Donegani, Eni S. p. A., via Fauser 4, 28200 Novara, Italy. E-mail: riccardo.po@eni.com*
[d] *Centro Nazionale per il Controllo e la Valutazione dei Farmaci, Istituto Superiore di Sanità, Viale Regina Elena, 299, 00161 Roma, Italy*
[e] *Istituto per lo Studio delle Macromolecole, Consiglio Nazionale delle Ricerche (ISMAC-CNR), Via E. Bassini, 15, 20133 Milano, Italy*

† Electronic supplementary information (ESI) available. See DOI: 10.1039/c7nj01501a

Published on 26 July 2017. Downloaded by Universita Studi di Milano on 6/8/2022 8:42:27 AM.

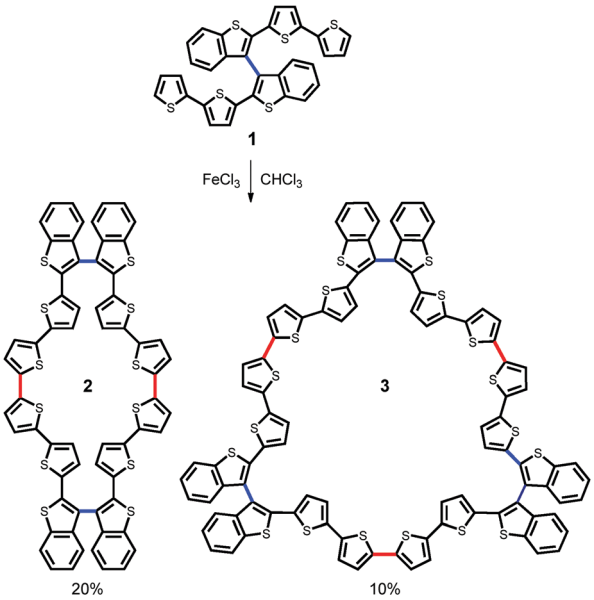

Scheme 1 2D representation of monomer **1**, cyclic dimer **2** and trimer **3**. Blue bonds contain the stereogenic axes, while red bonds are the connections between monomer **1** units.

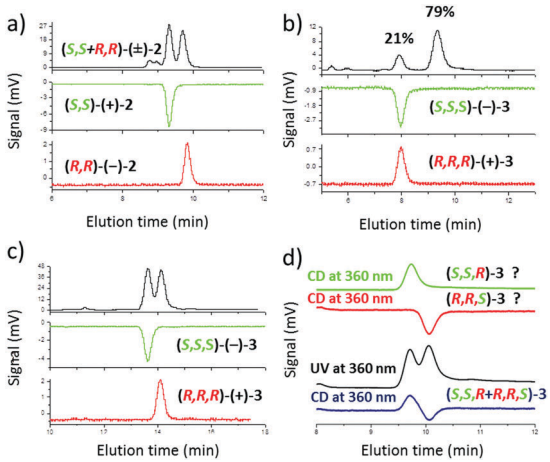

Fig. 1 (a) Analytical HPLC analysis on a CSP of cyclodimers **2** obtained by $FeCl_3$ oxidation of (±)-**1** in comparison with enantiopure samples of (*S*,*S*)-(+)-**2** (green) and (*R*,*R*)-(−)-**2** (red). Columns: Chiralpak IB-3 (250 mm × 4.6 mm I.D.) + Chiralpak IB-3 (100 mm × 4.6 mm I.D.); eluent: acetone : ethanol 100 : 60; flow rate: 1 mL min^{-1}; temperature: 5 °C; detector: UV (black) and CD (red/green) at 410 nm. (b) Analytical HPLC separation on an achiral SP of the two racemic diastereoisomers of **3** and confirmation that the first eluted product is the homochiral racemate by comparison with authentic enantiopure samples. Column: Nucleosil C18 (250 mm × 4.6 mm I.D.); eluent: acetone : ethanol 100 : 60; flow rate: 1 mL min^{-1}; temperature: 5 °C; detector: UV (black) and CD (red/green) at 410 nm. (c) Analytical HPLC resolution of the homochiral racemic trimers **3** and control of enantiomeric purity: (*S*,*S*,*S*)-(+)-**3** (green) and (*R*,*R*,*R*)-(−)-**3** (red); experimental conditions as described for (a). (d) Analytical HPLC resolution of the heterochiral racemic trimer **3** (below) and purity control of the separated enantiomers (above). Column: Chiralpak IB-3 (250 mm × 4.6 mm I.D.) eluent: acetone : ethanol 100 : 60; flow rate: 1 mL min^{-1}; temperature: 5 °C; detector: UV (black) and CD (red/green) at 360 nm.

cells are compared with those obtained using linear oligothiophenes as donor components in organic solar cells.[16,17]

We also compare the properties of cyclodimer **2** with those exhibited by the corresponding open-chain dimer **2a.** The latter was also employed as a starting material for the synthesis of the cyclic square-shaped tetramer **4**, which is a minor, but not negligible, component of the mixture of macrocycles resulting from $FeCl_3$ oxidation of **1**.

Results and discussion

Synthesis and structural characterization

The $FeCl_3$ oxidation of racemic (±)-**1** was carried out according to the described procedure.[11] After the usual work-up, a crude orange-red solid was obtained, which was extracted with THF in Soxhlet apparatus. The residue (50% yield) was composed of a mixture of cyclic stereoisomeric dimers **2** (67%, based on the highest peak intensity in High Resolution Laser Desorption Ionization (HRLDI) spectrum), trimers **3** (27%), tetramers **4** (2%) and the pentamers (less than 1%).

Careful column chromatography of this mixture allowed us to isolate cyclic dimers **2** and trimers **3** in a chemically pure state (HRLDI).

A couple of D_2 symmetric enantiomers and a C_{2h} symmetric *meso*-stereoisomer are expected for **2**, while two diastereomeric racemates, one D_3 symmetric – resulting from three homochiral (*R*,*R*,*R* and *S*,*S*,*S*) couplings – and one C_2 symmetric – generated by heterochiral (*R*,*R*,*S* and *S*,*S*,*R*) combinations – are expected for **3**.

Analytical HPLC experiments on a chiral stationary phase demonstrated that cyclodimeric compound **2** is exclusively constituted by the racemate. Indeed, we were able to resolve it into the antipodes that we had obtained and characterized starting from the single enantiomers of **1** (Fig. 1a). Unexpectedly, we did not find evidence for the formation of the *meso* diastereoisomer. This result is in agreement with the ^{1}H-NMR spectrum of the mixture, which was found to be superimposable on the spectrum of enantiopure (*R*,*R*)- or (*S*,*S*)-**2** (Fig. S1a, ESI†).

HPLC analysis of cyclotrimers **3** on the achiral stationary phase demonstrated that it is an about 4 : 1 mixture of the two expected diastereoisomeric racemates (Fig. 1b). Racemic samples of both diastereoisomers could be isolated in a chemically pure state using semi-preparative HPLC. We found that the minor component of the mixture of cyclotrimers **3** is the racemate of the C_3 symmetric diastereoisomer by comparison of the retention times with those shown by the enantiopure cyclotrimers obtained from the enantiopure antipodes of **1** (Fig. 1b).[11]

HPLC analysis of the two samples on a chiral stationary phase (CSP) succeeded in a partial, though not fully satisfactory, resolution (Fig. 1c and d).

For the moment, no data are available for the univocal configurational assignment to the three stereogenic axes of the two C_2 symmetric enantiomers (*R*,*R*,*S*)-**3** and (*S*,*S*,*R*)-**3**. A tentative assignment (Fig. 1d) was performed by considering that in this family of macrocycles, the *R* axis configuration generally increases the retention times over the *S* one, under the experimental

 This journal is © The Royal Society of Chemistry and the Centre National de la Recherche Scientifique 2017

Published on 26 July 2017. Downloaded by Universita Studi di Milano on 6/8/2022 8:42:27 AM.

conditions adopted for resolution and analytical check (Fig. 1a and c). According to this hypothesis, the first eluted stereoisomer would be (*S*,*S*,*R*)-**3**.

The ^{1}H-NMR spectrum of the mixture of cyclotrimers **3** and diastereoisomerically pure compounds confirmed the HPLC results (Fig. S1, ESI†).

A reasonable explanation for the diastereomeric distribution in cyclic dimers **2** and trimers **3** is based on the calculated preferred conformation of the radical cations of open chain dimer **2a** which are the precursors of both **2** and **3**.[18] The (*R*,*R*)- and (*S*,*S*)-**2a** stereoisomers display the two bithiophene terminals oriented on the same side, and thus prone to undergo intramolecular oxidative coupling giving a pair of enantiomers of **2** (Fig. 2a).

The conformational situation is very different in the case of the (*R*,*S*)-*meso*-**2a**, which is the only possible precursor of *meso*-**2** and of C_2 symmetric diastereoisomers of trimer **3**. In this case, the two bithiophene units extend along opposite directions (Fig. 2b): the intramolecular coupling affording the *meso* cyclodimer is strongly disfavored since it would require a too energetically demanding conformational rearrangement. Consequently, further coupling with a new molecule of **1** is easier and this would give an open-chain trimer in which the bithiophene extremities are again oriented in a favorable conformation for undergoing ring closure (Fig. 2c).

According to the research plan, we synthesized open-chain dimer **2a** and macrocyclic tetramer **4** (Scheme 2).

The former was prepared by using $CuCl_2$ as a promoting agent for the oxidative coupling of the mono anion of racemic **1**. HPLC analysis on CSP of the reaction mixture demonstrated that it consists of two enantiomers and the *meso* stereoisomer in a statistical 1 : 2 : 1 ratio (Fig. 3).

The square-shaped macrocycle **4** was synthesized through a $FeCl_3$-promoted cyclodimerization process of **2a** involving the unsubstituted α-positions of terminal thiophene units. As expected, the reaction products are oligomers containing an even number of monomeric units, *i.e.* dimer **2** (50%), tetramer **4** (46%), the hexamer (3%) and traces of the octamer (<1%), as can be seen in the HRLDI spectrum (Fig. S2, ESI†).

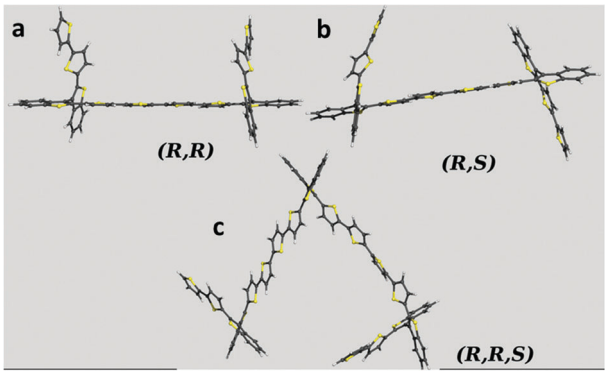

Fig. 2 Preferred calculated conformation for the radical cation of (*R*,*R*)-**2a** (a), of (*R*,*S*)-**2a** (b) and of open-chain (*R*,*R*,*S*)-trimer **3** (c).

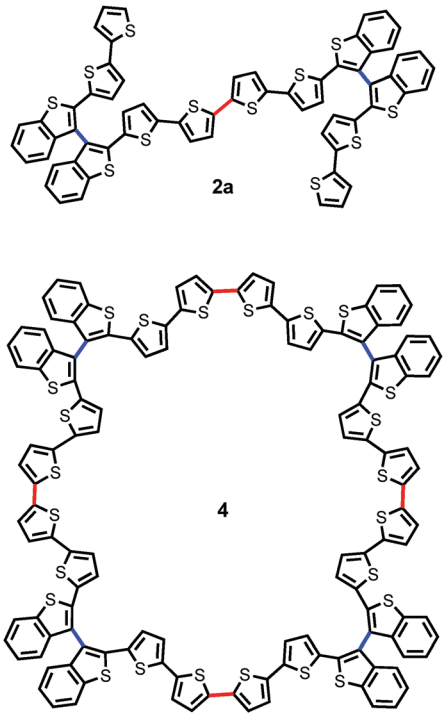

Scheme 2 Above: 2D representation of the open-chain dimer **2a**; below: macrocyclic square-shaped tetramer **4**. Blue bonds contain the stereogenic axes; red bonds are the connections between monomer 1 units.

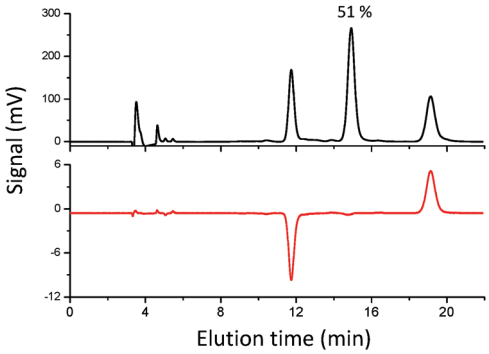

Fig. 3 HPLC chromatogram of **2a**. Column: Chiralpak IB (250 mm × 4.6 mm I.D.); eluent: *n*-hexane : dichloromethane : ethanol 100 : 10 : 2; flow rate: 1 mL min^{-1}; temperature: room temperature; detector: UV (black) and CD (red) at 360 nm.

The very poor solubility of **4** was an obstacle to its chromatographic purification. Nevertheless, **4** could be obtained in a reasonable degree of purity after six cycles of selective precipitation with *n*-hexane (3.5 mL) from filtered CH_2Cl_2 solution (1.5 mL) followed by centrifugation. The HRLDI spectrum of the material resulting after this treatment (Fig. S3, ESI†) confirms the complete absence of dimer **2**, while only traces of the hexamer are still present. Furthermore, the ^{1}H-NMR spectrum of **4** (Fig. S4, ESI†) confirms that dimers **2** and **2a** have been removed. Noteworthily, the broadness of the peaks observed for **4** is a consequence of the concomitant presence of several stereoisomers (two racemates and two *meso* compounds).

Published on 26 July 2017. Downloaded by Universita Studi di Milano on 6/8/2022 8:42:27 AM.

Photophysical characterization

The photophysical properties of the new oligomers **2a** and **4** are studied in comparison with those of the previously reported **2** and **3**,[11,19] under diluted conditions (1×10^{-5} M), in air equilibrated dichloromethane solution at room temperature. The corresponding spectra are depicted in Fig. 4 and the photophysical data are listed in Table 1.

The absorption spectrum of **4** displays a broad absorption band with a maximum at 452 nm, only 8 nm red-shifted with respect to that observed for **3**. Such absorption can be assigned to the spin-allowed π–π* transition involving the α-sexithiophene chains. The highest molar extinction coefficient observed in **4** is in agreement with this attribution even if this parameter is not linearly proportional to the number of sexithiophene chains constituting the different oligomers.

The same feature is observed also in the absorption spectrum of **2a**, which displays a low-energy absorption band at 458 nm, attributed to the π–π* transition of the six α-linked thiophene units. The further observed red-shift is in agreement with the higher degree of coplanarity, with consequent gain in the conjugation extent, due to the loss of steric constraints in the open chain oligomer. In contrast to what has been observed in the case of cyclic oligomers **2–4**, the open chain **2a** displays a higher energy absorption band at 382 nm which can be attributed to the π–π* transition involving the two lateral terthiophene units.

Upon optical excitation in the range of 410–450 nm, all the oligomers show intense and structured emission in the orange-yellow region of the visible spectrum, which is independent of the excitation, also for **2a**, attributed to the radiative decay of the π–π* excited state. The structured emission is in agreement with the planar quinoid-like structure proposed for the singlet excited states of the oligo-thiophenes.[20] The more planar conformation of **2a** is reflected also on the value of photoluminescence quantum yield (Φ). Indeed, while the Φ value of cyclic oligomer **4** is comparable to that measured for analogous oligomer **3** (0.32 for **4** *vs.* 0.37 for **3**)[11] in the case of **2a** this value is about 0.44 as a consequence of the absence of structural constraints that could favor the non-radiative decay pathway.

Table 1 Photophysical properties of compounds **2a–4** in air-equilibrated dilute CH_2Cl_2 solution at room temperature

	λ_{abs} (nm)	ε ($\times 10^4$ M^{-1} cm^{-1})	λ_{em} (nm)	Φ
2a	458 (382)	6.1 (6.8)	534–572	0.44
2	423[a]	5.3[a]	540–574	0.16[a]
3	447[a]	13[a]	541–579	0.37[a]
4	454	15	536–578	0.32

[a] Data already reported in ref. 11.

Electrochemical characterization

The electronic properties of oligomers **2a** and **2–4** have also been investigated by cyclic voltammetry (CV) on a GC electrode in CH_2Cl_2 + 0.1 M $TBAPF_6$. A synopsis of CV patterns recorded at a scan rate of 0.2 V s^{-1} is provided in Fig. 5; oxidation and reduction peak potentials are collected in Table 2 together with the corresponding estimated HOMO and LUMO energies and related energy gaps.

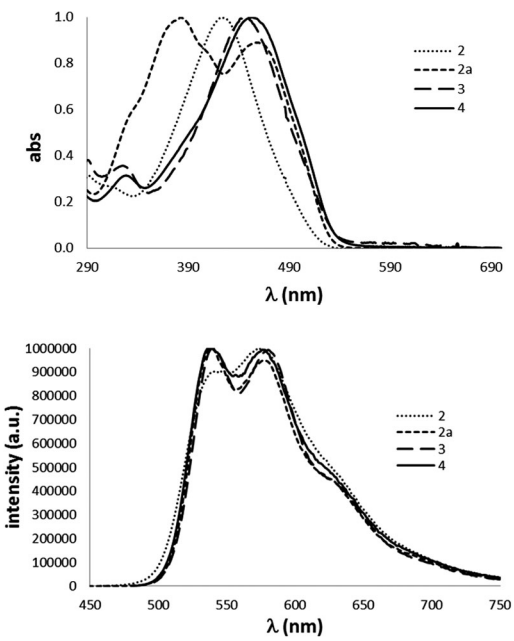

Fig. 4 UV-vis (top) and emission (bottom) spectra of **2**, **2a**, **3** and **4** oligothiophene compounds in air-equilibrated CH_2Cl_2 solution at room temperature.

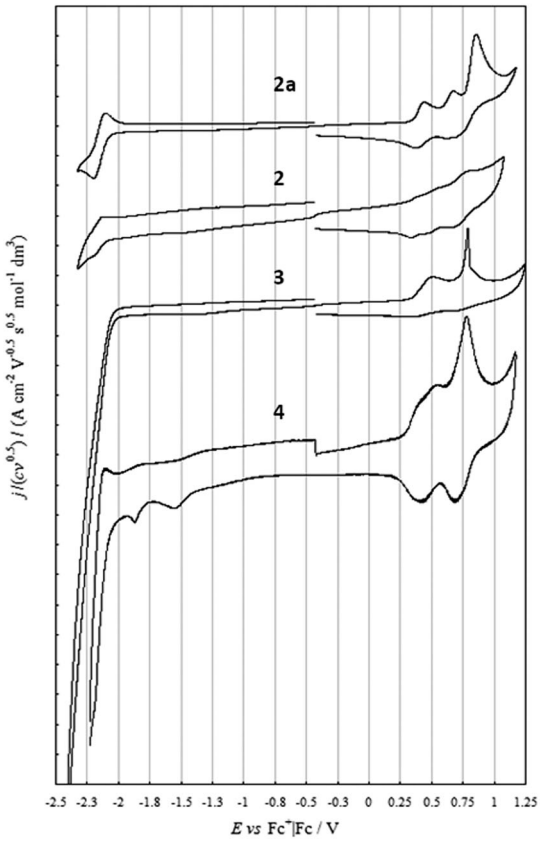

Fig. 5 CV patterns of oligomers **2a** and **2–4** on a GC electrode in CH_2Cl_2 + 0.1 M $TBAPF_6$ at 0.2 V s^{-1} scan rate.

Published on 26 July 2017. Downloaded by Universita Studi di Milano on 6/8/2022 8:42:27 AM.

Table 2 Oxidation and reduction peak potentials $E_{p,a}$ and $E_{p,c}$, referred to the $Fc^+|Fc$ couple, for oligomers **2a** and **2–4**, obtained on GC at 0.2 V s^{-1} in CH_2Cl_2 + 0.1 M $TBAPF_6$, and corresponding calculated HOMO and LUMO energies and gaps. For the sake of comparison, literature data are also reported for monomer **1** ($E_{p,a}$ in the same medium)[19] and for linear oligothiophenes $\mathbf{T_3}$, $\mathbf{T_4}$ and $\mathbf{T_6}$ (formal potentials $E^{\circ\prime}_{ox}$ in the same medium and $E^{\circ\prime}_{red}$ in DMA + TBABr),[13] all of them normalized *vs.* $Fc^+|Fc$

	$E_{p,c}$ (V)	$E_{p,a}$ (V)	LUMO (eV)	HOMO (eV)	E_g(electrochem) (eV)	E_g(optical) (eV)
$\mathbf{T_3}$	−2.5	0.58	−2.30	−5.38	3.08	3.50^{max}
	−2.9	1.53				
$\mathbf{T_4}$	−2.34	0.43	−2.46	−5.23	2.77	3.28^{max}
	−2.64	0.87				
	−3.68	1.94				
$\mathbf{T_6}$	−2.21	0.28	−2.59	−5.08	2.49	$2.87^{max\,b}$
	−2.36	0.50				
	−3.13	0.88				
1	n.d.	0.67		−5.47		$2.89^{onset\,a}$
		0.80				$3.34^{max\,a}$
2a	−2.20	0.45	−2.60	−5.25	$\sim 2.41^{onset}$	$2.33^{onset\,b}$
		0.68			2.65^{max}	$2.70^{max\,b}$
		0.86				
2	−2.12	0.39	−2.68	−5.19	$\sim 2.27^{onset}$	$2.36^{onset\,b}$
		0.54			2.51^{max}	$2.93^{max\,b}$
		0.79				
3	−2.20 (shoulder)	0.43	−2.60	−5.23	$\sim 2.39^{onset}$	$2.29^{onset\,b}$
		0.50 (sharp)			2.65^{max}	$2.77^{max\,b}$
		0.79				
4	−2.20	0.37	−2.60	−5.17	$\sim 2.33^{onset}$	2.73
		0.55				
		0.78			2.57^{max}	

[a] In CH_2Cl_2. [b] In toluene.

Open dimer **2a** (*meso* form and racemate in 1 : 1 ratio) shows three oxidation peaks in the available potential window, the first of which at 0.45 V ($Fc^+|Fc$), as well as a single reduction peak at −2.20 V, just before the negative background, consistent with the *p* character of this semiconductor family. The first oxidation peak potential is nearly constant with the scan rate, and has a half-peak width of about 57 mV, indicating a rather fast monoelectronic transfer. Moreover, the return peak, nearly symmetrical to the forward one (and improving with increasing scan rate), points to a rather stable product resulting from the electron transfer. Similar considerations also hold, although a bit less neatly, for the second oxidation peak. The third peak height, instead, is consistent with the global transfer of a higher number of electrons. Its lack of the return peak even at high scan rates and its scan rate dependency are consistent with a fast chemical follow up after an initial rather facile electron transfer step. On the whole, we can attribute the first system of twin reversible monoelectronic peaks to two subsequent oxidations (fast and leading to stable radical cations and dications, respectively) on the central hexathiophene chain, *i.e.* the conjugated system of highest efficiency, having no free terminals for oligomerization. Actually, the distance between the first and second oxidation peaks is nearly the same as in linear α-sexithiophene (Table 2).[13] Instead, the third oxidation must involve radical cation formation on the terthiophene terminals, with subsequent radical cation coupling processes, like in the case of the first oxidation of parent monomer **1**; the more positive oxidation potential of **2a** could be consistent with the repulsive interaction with the positive charges already present on the molecule. Concerning the chemical follow up, for the reasons previously discussed, we assume that it would be the ring closure of the chiral species to give racemic **2** or the addition of a new **2a** radical cation to give tetramer **4** and the corresponding open chain forms, which would evolve toward higher molecular weight oligomers.

The reduction peak features of **2** point to a facile and chemically reversible monoelectronic electron transfer, located of course on the central sexithiophene system.

On the oxidation side the CV behaviour of cyclodimer **2** recalls the electrochemical features shown by macrocyclic oligothiophenes containing two opposite β,β′-linkages.[9] Indeed three peaks are observed, all of them corresponding to fast electron transfers (the peak potentials being nearly constant with the scan rate) leading to stable charged products (according to the symmetrical return peaks). The first two peaks are at 0.15 V distance, approximately centred around the open dimer's first oxidation peak potential, with the third one following at about 0.25 V distance; the peak height ratio is 1 : 1 : 2. Taking into account that the presence of the *meso*-**2** cyclodimer (which, in principle, could behave differently from diastereoisomers (*R*,*R*)-**2** and (*S*,*S*)-**2**) has to be ruled out, two interpretations could be proposed for the three-peak system:

(a) first and second peak: monoelectronic oxidation of the two slightly interacting hexathiophene chains, at two slightly different potentials, as for two slightly interacting equivalent redox sites; third peak: second oxidation of the two chains, with merged peaks;

(b) three subsequent oxidations on each hexathiophene chain, similar to the linear sexithiophene oligomer $\mathbf{T_6}$ case (Table 2).

Assumption (a) looks more reasonable since in case (b) a 1 : 1 : 1 peak height ratio would be expected. Moreover, assumption (b) would imply an extremely high degree of molecule charging at low potentials. Furthermore, the peak distances are significantly different with respect to $\mathbf{T_6}$ (0.22 V and 0.38 V in $\mathbf{T_6}$ *vs.* 0.15 V and 0.25 V in the cyclic dimer **2**); actually this might be justified with a lower conjugation efficiency as a consequence of a less planar chain conformation of the hexathiophene chain in the cyclic dimer. However, in the same peculiar structure the global conjugation could also involve interactions between the two chains facing each other in space (besides some possible communication through the dibenzothiophene nodes, too) in line with very recent findings on macrocyclic oligothiophenes with stereogenic [2.2]*para*cyclophane scaffolds.[10]

Cyclotrimer **3** features three hexathiophene chains, partially connected through the dibenzothiophene nodes, and reciprocally more distant in space with respect to cyclodimers. Most cyclic trimers should have the (*R*,*R*,*S*) and (*S*,*S*,*R*) configuration and being enantiomers, they gave the same electrochemical response. The oxidative side of the CV pattern features two non-canonical systems at 0.5 and 0.8 V, *i.e.* at potentials similar to those of the first oxidation and the second oxidation in cyclodimers (according to assumption (a)); this looks quite reasonable, dealing with the same hexathiophene chains. Both signals show chemical reversibility if the scan is reversed immediately

Published on 26 July 2017. Downloaded by Universita Studi di Milano on 6/8/2022 8:42:27 AM.

after them at a sufficiently high scan rate; this is consistent with the absence of free terminals for oligomerization. The first signal is a wide peak which could correspond to the (nearly) merging of the first oxidation peaks of the three equivalent hexathiophene chains, being less interacting in space with respect to the dimer case. The second system, which should account for second oxidations, is dimensionally similar to the first one, but also features a peculiar sharp peak, quite reproducible, decreasing with increasing scan rate with respect to the main diffusive peak (unlike *e.g.* canonical adsorption peaks).

The CV pattern of cyclic tetramer **4** resembles that of cyclic dimers in the first system of two nearly merging peaks, and that of cyclic trimers in the second system including a sharp peak.

Cyclic dimers **2** has a significantly larger spectroscopic E_g than the open ones (2.93 *vs.* 2.70 eV), which might be justified in terms of lower conjugation efficiency on the hexathiophene chains as a consequence of structural constrictions in the cyclic molecule. However, the sequence is reversed for electrochemical data, *i.e.* E_g is significantly smaller for cyclodimers than for open chain dimers (2.51 *vs.* 2.65 eV), as a consequence of lower LUMO and higher HOMO levels (that is, both reduction and oxidation are more favoured). A tentative assumption might be in terms of stabilization of the (charged electron transfer product counteranion) couples by macrocycle complexation. The stabilizing effect of ionic couple formation with the electron transfer product resulting in milder reduction or oxidation potential, particularly in a low-polarity solvent, is well known in the literature.[21,22]

Cyclotrimers **3** have a significantly smaller spectroscopic E_g than cyclodimers (2.77 *vs.* 2.93 eV); this could be consistent with higher ring coplanarity in α-sexithiophene moieties and therefore higher conjugation efficiency in the larger macrocycle (like in open dimers, which have a similar gap, 2.70 eV). However, the sequence is reversed for electrochemical data, *i.e.* **3** has a larger gap than **2** (2.65 *vs.* 2.51 eV); would the above assumption of interanular interaction be correct, this might be justified in terms of a looser interaction in the larger macrocycle. Consistently, the difference in the E_g value decreases with increasing ring size: **3** and **4** exhibit nearly the same E_g values.

Bulk-heterojunction solar cells (BHJSCs)

The stereoisomeric mixtures of open chain **2a** and cyclic oligomers **2** and **3** have been tested separately as donors in bulk-heterojunction solar cells in combination with the acceptors commonly used in BHJSCs, namely C_{60} and PCBM.

A preliminary theoretical investigation has been performed in order to acquire elements useful to rationalize the experimental results.

Modelling. The C_{60} and PCBM fullerenes and the stereoisomers of **2a**, **2** and **3** oligothiophenes (Fig. S5, ESI†) have been separately modeled at 0 K, in a vacuum, with a simplified setup resulting in structures representative of the real geometries of the systems. These structures underwent refined geometrical optimization carried out using a more rigorous DFT approach, based on a combined BP-86/B3-LYP functional, using the Triple Zeta + Polarization Slater type orbital basis set. This is an acceptable compromise between computational cost and the need for using extended basis sets and strong exchange/correlation functionals to correctly estimate fine electronic properties. However, in order to identify the best computational method according to the limits described above, a preliminary systematic study of all the molecular systems has been performed. A set of extense computations has been performed applying different combinations of basis sets (DZP, TZP, TZ2P, *etc.*) and functionals (BP86, XLYP). Although the results are quantitatively different, they all remain in qualitative agreement with each other.

After the single molecule optimizations, the five models of the thiophene derivatives ((*R*,*R*)-**2a**, (*R*,*S*)-**2a**, (*R*,*R*)-**2**, (*R*,*R*,*R*)-**3** and (*R*,*R*,*S*)-**3**) have been juxtaposed to the two fullerene models (C_{60} and PCBM). For each interacting pair, a careful scan of the possible combinations of relative orientations and approach directions has been performed, followed by rigorous DFT optimization. This allowed us to identify the most stable oligothiophene-fullerene dyads (Fig. S6, ESI†).

Moreover, also the competing thiophene–thiophene and fullerene–fullerene pairs have been studied in order to evaluate the relative stability toward thiophene–fullerene couples: it was found that **2**:**2** adducts (−44 kcal mol^{-1}) are more stable than **3**:**3** ones (about −30 kcal mol^{-1}) and PCBM:PCBM pairs (−16 kcal mol^{-1}) are more stable than C_{60}:C_{60} ones (−8 kcal mol^{-1}).

Finally, an analysis of the delocalization of the frontier orbitals has been performed to evaluate the orbital overlap that could give rise to electron transfer processes.

Calculations showed that both C_{60} and PCBM fit in **2**, **3** and **2a** cavities giving stable dyads. The interaction involves mainly the HOMO and LUMO of each couple (Fig. 6) and the coordination enthalpy of the dyad increases with the number of thiophenes facing the fullerene surface. Dyads with fullerenes external to the thiophene oligomers are disfavored, although we cannot rule out that more complex interactions occur in a condensed phase environment.

The strength of the coordination enthalpy increases from **2** to **3** for both C_{60} and PCBM. In particular the coordination enthalpies of **2**:C_{60} couples are roughly equal to those of the corresponding **2**:PCBM couples, while for compound **3** they are lower for **3**:C_{60} than those for the **3**:PCBM dyad (Table 3). **3**-Based heteroadducts are more stable than the corresponding homoadduct, while the opposite is observed for **2**-based heteroadducts.

Due to their lower rigidity, open homologue **2a** seems to embrace more effectively the C_{60}/PCBM molecule resulting in a stronger stabilization of the dyad (about 5 kcal mol^{-1}) with respect to cyclic form **2**.

The stability of oligothiophene–fullerene couples, estimated by means of DFT calculations, gives an idea of the structural characteristics of the active layer of organic PV cells containing these materials and is helpful for the interpretation of the performances of the device.

Photovoltaic properties. The photovoltaic properties of cyclic oligothiophene:PCBM and cyclic oligothiophene:C_{60}, in solution-deposited (by spin coating) inverted solar cells, were investigated.

 This journal is © The Royal Society of Chemistry and the Centre National de la Recherche Scientifique 2017

Published on 26 July 2017. Downloaded by Universita Studi di Milano on 6/8/2022 8:42:27 AM.

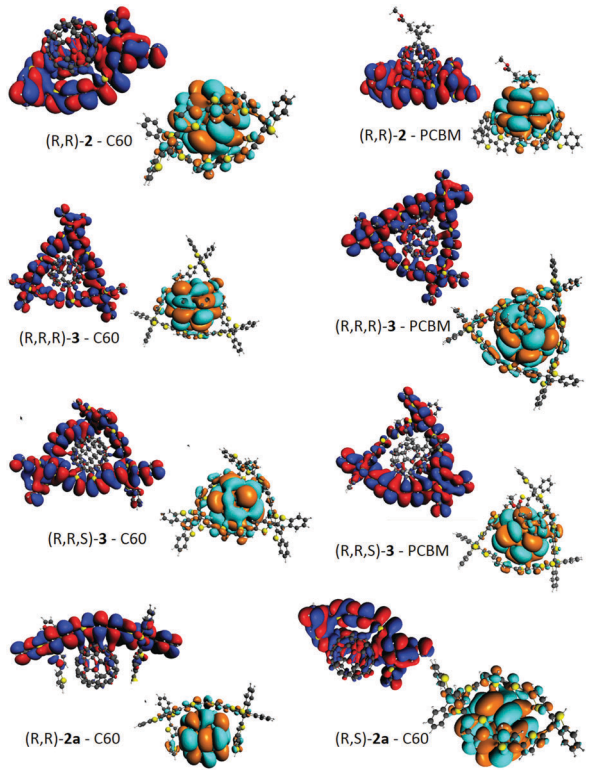

Fig. 6 Molecular orbitals (red-blue: HOMO; orange-cyan: LUMO) of oligothiophene:fullerene adducts.

The relatively poor solubility of unfunctionalized fullerene does not prevent a wet-deposition process of the active layers. Anyway, in several cases, the formation of aggregates (Fig. S7, ESI†) was observed as a possible consequence of the high tendency of oligothiophene to crystallize.

Reference devices with P3HT were also prepared. The donor : acceptor ratio was 1 : 1 wt/wt and a preliminary screening of a mixture of cyclic oligomers (Mix = **2** + **3**) was carried out to select the best solvent and the spinning conditions. Incidentally, it is worth noting that the choice of testing also the mixture was motivated by economic reasons. In fact, in this perspective the process leading to pure **2** or **3** oligomers is envisaged to be very expensive, because it involves a chromatographic separation. However, for the OPV technology to be cost-effective, scalable and widespread, the cost of the active materials has to be kept at a minimum, and column chromatographies have to be avoided whenever possible.[23–25]

Table 3 Interaction energy and frontier orbital energies of oligothiophene: fullerene dyads

Couple	Interaction enthalpy (kcal mol^{-1})	HOMO (eV)	LUMO (eV)
(*R*,*R*)-**2a**:C_{60}	−35.67	−4.34	−3.68
(*R*,*S*)-**2a**:C_{60}	−34.70	−4.35	−3.59
(*R*,*R*)-**2**:C_{60}	−30.16	−4.48	−3.71
(*R*,*R*,*R*)-**3**:C_{60}	−37.21	−4.39	−3.68
(*R*,*R*,*S*)-**3**:C_{60}	−41.29	−4.31	−3.54
(*R*,*R*)-**2**:PCBM	−29.14	−4.39	−3.57
(*R*,*R*,*R*)-**3**:PCBM	−45.97	−4.23	−3.39
(*R*,*R*,*S*)-**3**:PCBM	−36.09	−4.84	−4.18

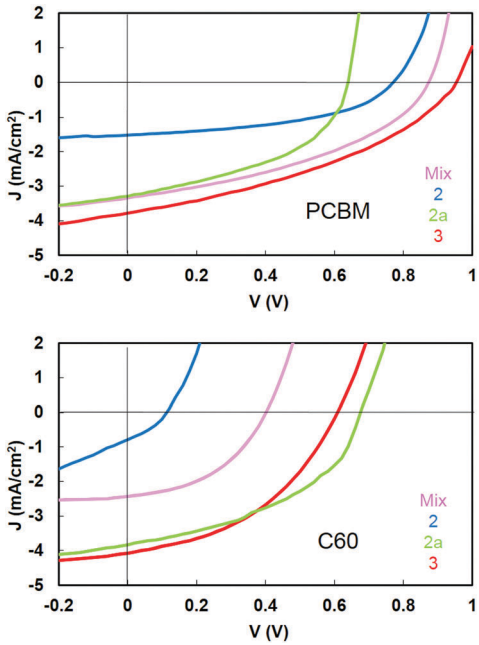

Fig. 7 *J*–*V* curves of oligothiophene:fullerene blends. Top: PCBM; bottom: C_{60}.

Virtually, no difference was observed among chlorobenzene and *o*-dichlorobenzene; thus, the latter was employed in the following experiments with a total concentration of donor + acceptor of 20 mg mL^{-1}. The best PCEs were obtained at a spinning speed of 1000 rpm. Thermal annealing (150 °C, 30 min) was found to be ineffective on the PCBM-based device performances and it has not been tested on C_{60}-based devices. The thicknesses of the active layer were generally around 40 nm, although its high roughness makes them difficult to measure (Fig. S7, ESI†).

The *J*–*V* curves of the polymer solar cells under AM 1.5 illumination at 100 mW cm^{-2} are shown in Fig. 7; photovoltaic parameters are summarized in Table 4. Average values and error bars are reported in the ESI† (Fig. S8).

Devices based on oligothiophene and the PCBM acceptor exhibit J_{sc}, FF and PCE lower than those of a P3HT:PCBM reference cell.

The J_{sc} value trend is consistent with the optical properties (*i.e.*, the absorption wavelength maxima, Fig. S9, ESI†) of the oligothiophene films. Their bad morphology (see the optical micrographs in the ESI,† Fig. S7) undoubtedly contributes to the deterioration of FF and J_{sc} (less than 4 mA cm^{-2} for the oligothiophenes, compared to 10.36 mA cm^{-2} for P3HT), besides affecting their reproducibility.

V_{oc} values do not reflect the trend of the HOMO levels of the oligothiophenes, because they are very likely affected by the aggregation of the blend components.[26,27] Among the oligomers, the mixture of stereoisomeric trimers **3** exhibits the highest PCE (about 1.1%), while that of cyclic dimers **2** leads to a PCE of about 0.3%. The PCE value of the oligomer mixture (Mix) is in between this close to the trimer, *i.e.* the most effective component. EQE curves substantially confirm the picture (Fig. 8).

Published on 26 July 2017. Downloaded by Universita Studi di Milano on 6/8/2022 8:42:27 AM.

Table 4 Photovoltaic parameters of oligothiophene:fullerene solar cells (maximum values in parenthesis)

Device	J_{sc} (mA cm^{-2})	V_{oc} (V)	FF	PCE (%)
P3HT:PCBM	10.13(10.36)	0.56(0.56)	0.57(0.57)	3.3 ± 0.1(3.30)
Mix:PCBM	3.16(3.35)	0.86(0.87)	0.41(0.41)	1.1 ± 0.1(1.20)
3:PCBM	3.74(3.78)	0.72(0.88)	0.39(0.41)	1.1 ± 0.2(1.40)
2:PCBM	1.43(1.52)	0.43(0.77)	0.44(0.47)	0.3 ± 0.1(0.55)
2a:PCBM	3.13(3.29)	0.42(0.64)	0.43(0.46)	0.6 ± 0.2(0.96)
P3HT:C_{60}	1.96(2.19)	0.42(0.42)	0.50(0.52)	0.4 ± 0.1(0.49)
Mix:C_{60}	2.38(2.43)	0.34(0.40)	0.41(0.45)	0.3 ± 0.1(0.40)
3:C_{60}	3.94(4.07)	0.42(0.61)	0.41(0.43)	0.7 ± 0.2(1.07)
2:C_{60}	0.44(0.79)	0.05(0.11)	0.11(0.34)	0.01(0.03)
2a:C_{60}	3.77(3.84)	0.56(0.67)	0.39(0.44)	0.8 ± 0.2(1.15)

A careful observation of the optimized model geometries shows that **2** models are not able to fully embrace the fullerene sphere but effectively enclose only one hemisphere. This results in a poor interaction energy compared with that obtained with **3** models, which effectively fully embrace the fullerene sphere. This is also in agreement with the low coordination enthalpy (Table 3) and the preferential formation of **2**:**2** homoadducts that should reasonably translate in a less efficient electron transfer process.

Interestingly, open-chain dimer **2a** has both PCE and EQE greater than those shown by cyclic dimer **2**. The comparison between open and closed forms shows that the first molecule stretches out over the fullerene easier than the latter. This is due to the lower degrees of geometrical freedom intrinsic in closed models with respect to the open ones.

Concerning the C_{60}-based devices, it is well-known that the acceptor performances of unfunctionalized fullerenes in polymer solar cells are worse than that of PCBM,[28–33] due to their lower solubility,[34,35] greater tendency to aggregation and poor filmability. A similar behavior has been observed with the oligothiophenes presented herein, with the exception of solar cells containing **2a** and **3**, which afford PCE values above that measured for the P3HT:C_{60} reference cell. This unexpected behavior can be ascribed to a fair acceptor dispersion that produces a morphology suitable for charge carrier transport and provides acceptable J_{sc} values. It can be speculated that the dispersion of C_{60} is facilitated by its envelopment in **3** or **2a** structures, as suggested by simulations (Fig. S5, ESI†). In the case of **2a**, the oligomer is probably able to tweeze the fullerene sphere through aromatic stacking interactions.[36] The same phenomenon partially occurs with the oligomer mixture Mix, where the presence of about 30% of **3** limits aggregation.

Comparing the OM of the cells prepared with PCBM and C_{60}, the presence of aggregates supports different PCE values. In particular, **Mix**:C_{60} performs better than **Mix**:PCBM; **3** behaves better with PCBM than with C_{60}, while **2a** behaves better than **2** in combination with both acceptors.

As previously noted for the **2**:PCBM system, also for the **2**:C_{60} blend the low J_{sc} might arise from a poor interaction as theoretically suggested by the low coordination enthalpy (Table 3).

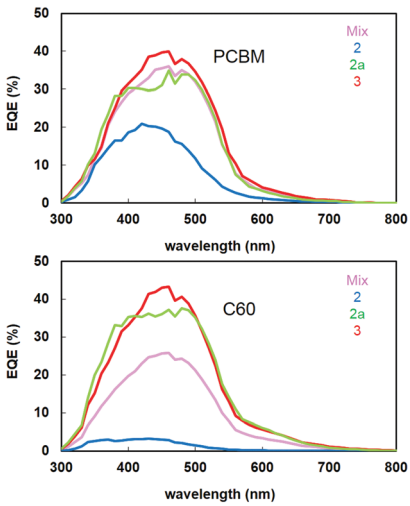

Fig. 8 External quantum efficiency spectra of oligothiophene:fullerene blends. Top: PCBM; bottom: C_{60}.

Experimental

Materials

All the reagents and solvents, including PCBM and C_{60}, were purchased from Sigma-Aldrich and used as received without further purification. P3HT (Plexcore OS 2100) has been provided by Plextronics Inc. $CHCl_3$ has been dried over P_2O_5 and distilled prior to its use.

The synthesis of cyclic oligomers **2** and **3** has been performed as previously described.[11]

Synthesis of the stereoisomeric mixture of 2a

n-BuLi 1.6 M solution in *n*-hexane (600 μL, 0.96 mmol) was added dropwise under an argon atmosphere to a solution of (±)-**1** (500 mg, 0.84 mmol) in dry THF (25 mL) and freshly distilled TMEDA (250 μL, 1.68 mmol) under stirring at −78 °C in 30 minutes. Within this time the mixture became dark orange. Then, solid $CuCl_2$ (340 mg, 2.53 mmol) was added and the mixture was allowed to warm up to room temperature and stirred for 20 hours. The solvent was evaporated under reduced pressure and the residue was dissolved in CH_2Cl_2 and washed with 1 M HCl and water. The organic layer was dried (Na_2SO_4), filtered and evaporated to dryness. The obtained orange brown solid was purified by column chromatography (THF/hexane-4 : 6) to give the stereoisomeric mixture (racemate/mesoform) **2a** in the pure state (141.2 mg, 0.119 mmol, yield 28%).

^{1}H NMR (500 MHz, CD_2Cl_2, 300 K): δ (ppm) = 7.96 (d, ^3J (H,H) = 8.8 Hz, 4H), 7.41 (t, ^3J (H,H) = 7.4 Hz, 4H), 7.28 (t, ^3J (H,H) = 7.4 Hz, 4H), 7.15–7.24 (m, 10H), 7.03–6.92 (m, 10H), 7.29 (d, ^3J (H,H) = 3.8 Hz, 2H).

^{13}C NMR (7.0 T, CD_2Cl_2, 40 °C): δ (ppm) = 140.76 (C), 140.73 (C), 139.30 (C), 138.75 (C), 138.66 (C),137.26 (C), 137.10 (C), 136.92 (C), 136.41 (C), 139.99 (C), 134.96 (C), 134.69 (C), 128.18 (CH), 127.73 (CH), 127.64 (CH), 125.76 (CH), 125.73 (CH), 125.42 (CH), 125.29 (CH), 125.07 (CH), 124.77 (CH), 124.39

Published on 26 July 2017. Downloaded by Universita Studi di Milano on 6/8/2022 8:42:27 AM.

(CH), 124.11 (CH), 124.05 (CH), 123.09 (CH), 123.04 (CH), 122.53 (CH).

Synthesis of the stereoisomeric mixture of 4

A solution of the stereoisomeric mixture **2a** (140 mg, 0.118 mmol) in dry $CHCl_3$ (20 mL) was added dropwise under an argon atmosphere into a slurry of $FeCl_3$ (90 mg, 0.55 mmol) in dry $CHCl_3$ (180 mL), under stirring, at room temperature, within 2 hours. The dark purple mixture was stirred overnight, then the volume of the solvent was reduced to 70 mL by evaporation under reduced pressure and the remaining solution was poured into MeOH (150 mL). The mixture became bright orange, and the precipitate was recovered by filtration and suspended in MeOH (30 mL), then hydrazine (4 drops) was added. The orange-red solid (130 mg) was recovered by filtration and extracted with THF using a Soxhlet apparatus, affording a soluble residue (81 mg) composed of cyclic oligomers of **1** with an even number of monomeric units (**2** = 50%, **4** = 46%, hexamers = 3%, octamers < 1%, HRLDI Fig. S2, ESI†). The solid (40 mg) was dissolved in CH_2Cl_2 (20 mL), the suspension was filtered to remove insoluble hexamers and octamers, and the resulting solution was concentrated to 3 mL. *n*-Hexane (7 mL) was added to the solution and the orange solid was collected after centrifugation. This procedure was repeated 6 times to give **4** in the pure state (12.0 mg, yield: 17%, HRLDI Fig. S3, ESI†). The mother liquors contained decreasing amounts of previously described **2**.

^{1}H NMR (400 MHz, CD_2Cl_2, 300 K): δ (ppm) = 8.13 (m, 8H), 7.44 (m, 8H), 7.27 (m, 16H), 7.18 (m, 24H), 7.08 (m, 8H), 6.98 (m, 8H).

HPLC

HPLC analyses were performed by using stainless steel Chiralpak IB-3 (250 mm × 4.6 mm i.d. and 100 mm × 4.6 mm i.d.), Chiralpak IB (250 mm × 4.6 mm i.d.) (Chiral Technologies Europe, Illkirch, France) and Nucleosil C18 (250 mm × 4.6 mm i.d.) (Sigma-Aldrich) columns. All solvents for HPLC were purchased from Sigma-Aldrich and used without further purification.

The analytical HPLC apparatus consisted of a PerkinElmer 200 LC pump equipped with a Rheodyne injector, a 200 μL sample loop, a HPLC Dionex CC-100 oven and a Jasco Model CD 2095 Plus UV/CD detector. The signal was acquired and processed using the Clarity software of DataApex.

Photophysical characterization

Photophysical measurements were carried out in air-equilibrated CH_2Cl_2 solutions at room temperature. Electronic absorption spectra were recorded on an Agilent Model 8543 spectrophotometer at room temperature, using quartz cells with 1.0 cm path length.

Steady-state emission spectra were recorded on an Edinburgh FLS980 spectrometer equipped with a 450 W ozone-free xenon arc lamp, double grating excitation and emission monochromators (2 × 300 mm focal length) and a Hamamatsu R928P photomultiplier tube.

Φ were collected on optically diluted solution ($<1.0 \times 10^{-5}$ M) using wavelength scanning with a Hamamatsu C11347-11 Quantaurus-QY Absolute PL quantum yield spectrometer, equipped with a xenon light source (150 W), a monochromator, a Spectralon integrating sphere, and employing the commercially available U6039-05 PLQY measurement software (Hamamatsu Photonics Ltd, Shizuoka, Japan).

Electrochemistry

The oligomers ((5×10^{-4} M in CH_2Cl_2, Aldrich, anhydrous, >99.8%) and 0.1 M, $TBAPF_6$, (Aldrich, purity, >98.0%)) were characterised by cyclic voltammetry, CV, at scan rates typically ranging from 0.02 to 2 V s^{-1}, using an Autolab PGSTAT potentiostat of Eco-Chemie (Utrecht, The Netherlands), run by a PC with the GPES software of the same manufacturer. The minicell (3 cm^3 working volume) included as the working electrode a glassy carbon (GC) disk embedded in glass (~0.031 cm^2, Metrohm), polished with a diamond powder of 1 μm diameter (Aldrich) on a wet DP-Nap cloth (Struers), as the counter electrode a Pt disk, as the operating reference electrode an aqueous saturated calomel electrode (SCE) in a double bridge, filled with the working medium, to avoid water and KCl leakage into the working solution; the working electrode potentials were afterwards referred to the formal potential $E^{\circ\prime}$ of the $Fc^+|Fc$ intersolvental reference redox couple measured under the same conditions. Solutions were deaerated by N_2 purging before each experiment, the cell being equipped with a pre-saturator to grant constant working volume.

Modelling

The modelling of cyclic oligothiophene:fullerene dyads has been obtained using Density Functional Theory (DFT).[37–39] A combined BP-86/B3-LYP functional using the Triple ZetaPolarization Slater type orbital basis set was applied.

Theoretical exploitation of weak bond interactions between fullerenes and thiophene moieties required the introduction of dispersion corrected DFT. The Grimme DFT-D3 method[40] was the natural choice due to its recognized ability to efficiently correct the well-known underestimation of π-interactions using standard hybrid DFT.

This methodology made it possible to obtain an acceptable theoretical estimation of the total formation energy of each dyad and of their interaction energies, together with the energies of each molecular orbital, including the frontier orbitals HOMO, and LUMO.

Fabrication of photovoltaic devices

Inverted solar cells were fabricated by first spin-coating 30 nm of sol–gel ZnO precursor[41] on top of ITO-coated glass substrates at 600 rpm for 150 s and annealed at 140 °C for 5 minutes. The active layer (~40 nm) was spin-coated at 1000 rpm for 90 s on top of ZnO from solution in *o*-dichlorobenzene heated at 60 °C. The total concentration of the active components was 20 mg mL^{-1}. 10 nm of MoO_3 buffer layer anode was deposited in a thermal evaporator in a vacuum of 10^{-6} mbar and the devices were completed by the deposition of 100 nm of silver. Each substrate contained three cells, with a nominal active area of 25 mm^2 each.

Published on 26 July 2017. Downloaded by Universita Studi di Milano on 6/8/2022 8:42:27 AM.

Testing of photovoltaic devices

Film thicknesses were measured on a Veeco Dektat 150 profiler. Current–voltage characteristics were measured in air by using a Keithley 2602A sourcemeter. Light intensity of 1.5 AM sunlight from an Abet 2000 solar simulator was calibrated using a KG-5 filtered Si photodiode. Inverted solar cells were illuminated through a 4×4 mm^2 area shadow mask. External quantum efficiencies (EQEs) were characterized using a Schreder GmbH (Kirchbichl, AT) system equipped with a Bentham TMc 300 and a certified mc-Si diode in which the monochromatic light was generated from a dual light source (Xe 150 W lamp and QH 100 W lamp). The spot diameter was 1 mm.

Optical microscopy

The active blend films were examined by using standard light microscopy (Nikon Eclipse LV150). All images were taken in air and at room temperature.

Conclusions

In this work, the distribution of macrocyclic stereoisomers obtained by the $FeCl_3$ promoted oxidation of racemic monomer **1** has been presented and explained. The interpretation holds on the analysis of the open dimer's and open trimer's radical cation geometry. Furthermore, open dimer **2a** and macrocyclic tetramer **4** have been synthesized and characterized.

The electrochemistry of the cyclic oligomers looks quite attractive on account of facile, reversible electron transfers as well as of possible 3D interactions between equivalent redox centers on reciprocally facing hexathiophene chains of macrocyclic systems.

The macrocyclic (**2** and **3**) and tweeze-shape (**2a**) oligomers have been tested as donor components in BHJSC in combination with C_{60} or PCBM. The results of the preliminary experiments give very interesting indications on the strategies that should be adopted for the design of these kinds of materials.

Although the results obtained with C_{60} and PCBM appear significantly different between them, EQE values are not always lower than those obtained using the classical reference system based on the P3HT:PCBM blend. Furthermore we can assert that those oligothiophenes able to effectively embrace the acceptor produce solar cells with better efficiencies. As a matter of fact, cyclic dimers **2** seems to be inappropriate to host fullerenes because they have a cavity too small for efficient donor–acceptor interactions. More favorable, however, is the situation for trimers **3** that can allocate fullerenes without fully incorporating them. Promising results in terms of efficiencies are achieved also for the tweeze-shape dimeric system **2a** although it is composed 50% of the *meso* form that has a zig-zag geometry.

We can conclude that the present work gives some useful indications for the architectural design of cyclic and bended macromolecules to be employed as donor components in the active layer of efficient solar cell devices.

Acknowledgements

The authors are grateful to professor Francesco Sannicolò (Università degli Studi di Milano, Dipartimento di Chimica) for fruitful discussion with the contribution from Fondazione Cariplo (Materiali avanzati 2011-0417 "Inherently Chiral Multifunctional Conducting Polymers"). The use of instrumentation purchased through the Regione Lombardia – Fondazione Cariplo joint SmartMatLab Project (2013-1766) is gratefully acknowledged.

Notes and references

1 J. Krömer, I. Rios-Carreras, G. Fuhrmann, C. Musch, M. Wunderlin, T. Debaerdemaeker, E. Mena-Osteritz and P. Bäuerle, *Angew. Chem., Int. Ed.*, 2000, **39**, 3481–3486.
2 F. Zhang, G. Götz, H. D. F. Winkler, C. A. Schalley and P. Bäuerle, *Angew. Chem., Int. Ed.*, 2009, **48**, 6632–6635.
3 F. Zhang, G. Götz, E. Mena Osteritz, M. Weil, B. Sarkar, W. Kaim and P. Bäuerle, *Chem. Sci.*, 2011, **2**, 781–784.
4 E. Mena-Osteritz, F. Zhang, G. Götz, P. Reineker and P. Bäuerle, *Beilstein J. Nanotechnol.*, 2011, **2**, 720–726.
5 M. Iyoda, K. Tanaka, H. Shimizu, M. Hasegawa, T. Nishinaga, T. Nishiuchi, Y. Kunugi, T. Ishida, H. Otani, H. Sato, K. Inukai, K. Tahara and Y. Tobe, *J. Am. Chem. Soc.*, 2014, **136**, 2389–2396.
6 H. Ito, Y. Mitamura, Y. Segawa and K. Itami, *Angew. Chem., Int. Ed.*, 2015, **54**, 159–163.
7 E. Mena-Osteritz and P. Bäuerle, *Adv. Mater.*, 2006, **18**, 447–451.
8 E. Mena-Osteritz, *Adv. Mater.*, 2002, **14**, 609–616.
9 K. Asai, A. Fukazawa and S. Yamaguchi, *Chem. Commun.*, 2015, **51**, 6096–6099.
10 M. Hasegawa, K. Kobayakawa, H. Matsuzawa, T. Nishinaga, T. Hirose, K. Sako and Y. Mazaki, *Chem. – Eur. J.*, 2017, **23**, 3267–3271.
11 F. Sannicolò, P. R. Mussini, T. Benincori, R. Cirilli, S. Abbate, S. Arnaboldi, S. Casolo, E. Castiglioni, G. Longhi, R. Martinazzo, M. Panigati, M. Pappini, E. Quartapelle Procopio and S. Rizzo, *Chem. – Eur. J.*, 2014, **20**, 15298–15302.
12 F. Sannicolò, P. R. Mussini, T. Benincori, R. Martinazzo, S. Arnaboldi, G. Appoloni, M. Panigati, E. Quartapelle Procopio, V. Marino, R. Cirilli, S. Casolo, W. Kutner, K. Noworyta, A. Pietrzyk-Le, Z. Iskierko and K. Bartold, *Chem. – Eur. J.*, 2016, **22**, 10839–10847.
13 K. Meerholz and J. Heinze, *Electrochim. Acta*, 1996, **41**, 1839–1854.
14 J. Heinze, B. A. Frontana-Uribe and S. Ludwigs, *Chem. Rev.*, 2010, **110**, 4274–4771.
15 S. Arnaboldi, T. Benincori, R. Cirilli, S. Grecchi, L. Santagostini, F. Sannicolò and P. R. Mussini, *Anal. Bioanal. Chem.*, 2016, **408**, 7243–7254.
16 J. Sakai, T. Taima and K. Saito, *Org. Electron.*, 2008, **9**, 582–590.
17 J. Sakai, T. Taima, T. Yamanari and K. Saito, *Sol. Energy Mater. Sol. Cells*, 2009, **93**, 1149–1153.
18 G. Longhi, S. Abbate, G. Mazzeo, E. Castiglioni, P. R. Mussini, T. Benincori, R. Martinazzo and F. Sannicolò, *J. Phys. Chem. C*, 2014, **118**, 16019–16027.

 This journal is © The Royal Society of Chemistry and the Centre National de la Recherche Scientifique 2017

Published on 26 July 2017. Downloaded by Universita Studi di Milano on 6/8/2022 8:42:27 AM.

19 F. Sannicolò, S. Arnaboldi, T. Benincori, V. Bonometti, R. Cirilli, L. Dunsch, W. Kutner, G. Longhi, P. R. Mussini, M. Panigati, M. Pierini and S. Rizzo, *Angew. Chem., Int. Ed.*, 2014, **53**, 2623–2627.
20 M. Takayanagi, T. Gejo and I. Hanazaki, *J. Phys. Chem.*, 1994, **98**, 12893–12898.
21 L. Holleck and D. Becher, *J. Electroanal. Chem.*, 1962, **4**, 321–331.
22 M. Magni, A. Colombo, C. Dragonetti and P. R. Mussini, *Electrochim. Acta*, 2014, **141**, 324–330.
23 R. Po, G. Bianchi, C. Carbonera and A. Pellegrino, *Macromolecules*, 2015, **48**, 453–461.
24 R. Po and J. Roncali, *J. Mater. Chem. C*, 2016, **4**, 3677–3685.
25 J. Min, Y. N. Luponosov, C. Cui, B. Kan, H. Chen, X. Wan, Y. Chen, S. A. Ponomarenko, Y. Li and C. J. Brabec, *Adv. Energy Mater.*, 2017, DOI: 10.1002/aenm.201700465.
26 K. Vandewal, S. Himmelberger and A. Salleo, *Macromol.*, 2013, **46**, 6379–6387.
27 B. Qi and J. Wang, *J. Mater. Chem.*, 2012, **22**, 24315–24325.
28 S. Rait, S. Kashyap, P. K. Bhatnagar, P. C. Mathur, S. K. Sengupta and J. Kumar, *Sol. Energy Mater. Sol. Cells*, 2007, **91**, 757–763.
29 K. Tada and M. Onoda, *Sol. Energy Mater. Sol. Cells*, 2012, **100**, 246–250.
30 D. E. Motaung, G. F. Malgas, C. J. Arendse, S. E. Mavundla, C. J. Oliphant and D. Knoesen, *Sol. Energy Mater. Sol. Cells*, 2009, **93**, 1674–1680.
31 C. Carati, N. Gasparini, S. Righi, F. Tinti, V. Fattori, A. Savoini, A. Cominetti, R. Po, L. Bonoldi and N. Camaioni, *J. Phys. Chem. C*, 2016, **120**, 6909–6919.
32 N. Gasparini, S. Righi, F. Tinti, A. Savoini, A. Cominetti, R. Po and N. Camaioni, *ACS Appl. Mater. Interfaces*, 2014, **6**, 21416–21425.
33 A. Cominetti, A. Pellegrino, L. Longo, A. Tacca, R. Po, C. Carbonera, M. Salvalaggio, M. Baldrighi and S. V. Meille, *Mater. Chem. Phys.*, 2015, **159**, 46–55.
34 Y. Marcus, A. L. Smith, M. V. Korobov, A. L. Mirakyan, N. V. Avramenko and E. B. Stukalin, *J. Phys. Chem. B*, 2001, **105**, 2499–2506.
35 R. S. Ruoff, D. S. Tse, R. Malhotra and D. L. Lorents, *J. Phys. Chem.*, 1993, **97**, 3379–3383.
36 A. Sygula, F. R. Fronczek, R. Sygula, P. W. Rabideau and M. M. Olmstead, *J. Am. Chem. Soc.*, 2007, **129**, 3842–3843.
37 R. G. Parr and W. Yang, *Density-Functional Theory of Atoms and Molecules*, Oxford University Press, New York and Oxford, 1989.
38 C. Fonseca Guerra, O. Visser, J. G. Snijders, G. teVelde and E. J. Baerends, in *METECC-95 STEF*, ed. E. Clementi and C. Corongiu, Cagliari, 1995, pp. 303–395.
39 G. teVelde, F. M. Bickelhaupt, E. J. Baerends, S. J. A. van Gisbergen, C. Fonseca Guerra, J. G. Snijders and T. Ziegler, *J. Comput. Chem.*, 2001, **22**, 931–967.
40 S. Grimme, J. Anthony, S. Ehrlich and H. J. Krieg, *J. Chem. Phys.*, 2010, **132**, 154104.
41 R. Po, A. Bernardi, A. Calabrese, C. Carbonera, G. Corso and A. Pellegrino, *Energy Environ. Sci.*, 2014, **7**, 925–943.